Directional grid maps: modeling multimodal angular uncertainty in dynamic environments

Ransalu Senanayake[1] and Fabio Ramos[1].

Abstract— **Robots often have to deal with the challenges of operating in dynamic and sometimes unpredictable environments. Although an occupancy map of the environment is sufficient for navigation of a mobile robot or manipulation tasks with a robotic arm in static environments, robots operating in dynamic environments demand richer information to improve robustness, efficiency, and safety. For instance, in path planning, it is important to know the direction of motion of dynamic objects at various locations of the environment for safer navigation or human-robot interaction. In this paper, we introduce directional statistics into robotic mapping to model circular data. Primarily, in collateral to occupancy grid maps, we propose *directional grid maps* to represent the location-wide long-term angular motion of the environment. Being highly representative, this defines a probability measure-field over the longitude-latitude space rather than a scalar-field or a vector-field. Withal, we further demonstrate how the same theory can be used to model angular variations in the spatial domain, temporal domain, and spatiotemporal domain. We carried out a series of experiments to validate the proposed models using a variety of robots having different sensors such as RGB cameras and LiDARs on simulated and real-world settings in both indoor and outdoor environments.**

I. INTRODUCTION

Safe operation of robots in dynamic environments where humans, vehicles, and other robots operate is central for full autonomy. Spatial information alone is not sufficient in complex environments. This is because, the prediction of future events drives decision making whilst properly managing the risk of collisions. Although conventional mapping techniques represent the space in terms of the probability of occupancy [1], [2], they do not explicitly capture the patterns in the motion direction of dynamic objects such as people, cars, and cyclists. Understanding and modeling directions are complicated and cannot be treated with conventional techniques from linear statistics as the treatment of angular quantities requires that distributions be mapped into hyperspheres, in a set of techniques known as directional statistics [3].

In general, a robot requires a map for path planning and safe navigation. To this end, the most common approach is to represent the actual geometry of the environment as floor plans [1] or 3D models [4], [5] in the metric space, though graph based approaches also exist [6]. These metric maps are typically built using data collected from RGB cameras or depth sensors such as LiDAR [1], [7].

The basic information about the environment a robot requires to maneuver is to know which areas of the envi-

[1]Authors are affiliated with the School of Information Technologies, and Centre for Translational Data Science, The University of Sydney, Australia; and Data61/CSIRO, Australia. Emails: rsen4557@uni.sydney.edu.au
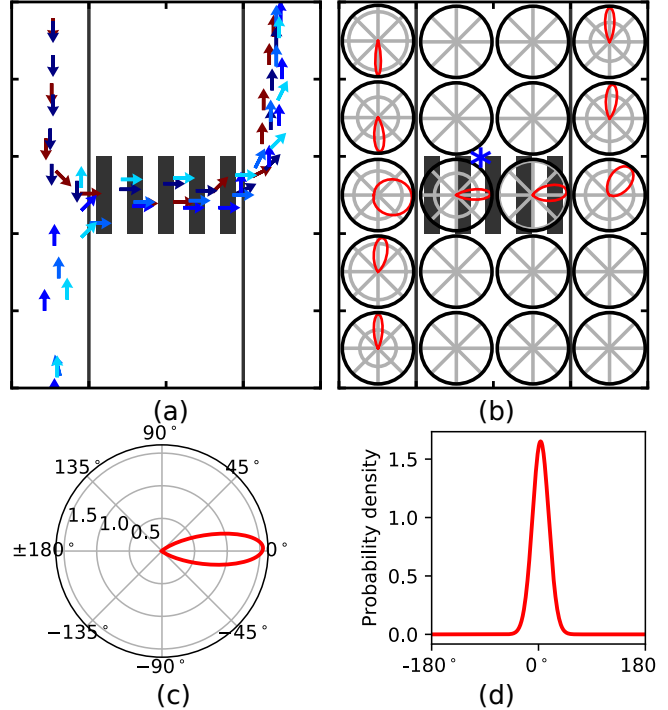
Fig. 1: Motivation for directional mapping. (a) Plan view of a road where simulated human coming from two directions walk across a crosswalk and head towards a different direction. We are interested in modeling directions people move after taking observations over a period of time (b) The world is divided in to a 5×4 grid. The *directional distribution*—a probability distribution over directions $[-180°, 180°]$—at different cells modeled using the proposed method (DGM) is illustrated using polar plots. For any location/cell in the space, such a directional distribution exists. The correspondence between the direction of arrows and the direction of polar plots can be observed. (c) To elaborate, the polar plot marked in $*$ on the grid map is emphasized. This shows the probability density for different angles at the particular cell—the probability density increases as go farther away from the center. (d) The equivalent unwrapped probability function with a support $[-180°, 180°]$ is given for clarity.

ronment are occupied and which areas are not. To model this, in his seminal paper, Elfes [1] proposed occupancy grid maps—the environment is divided into a grid and occupancy probability of each cell is updated as beam reflections are collected from a depth sensor such as sonar or LiDAR. Later, continuous scalar-field representations have been proposed [2], [8]. However, all of these methods assumed a static environment where the only moving object in the environment is the robot. To build a static occupancy map in the presence of a few dynamic objects, [9], [10] proposed to filter dynamic objects as a preprocessing step and then map the occupancy.

More recently, rather than considering dynamic objects as nuisances, they have been incorporated into the map in order

to model the long-term occupancy [11]–[14] and understand occupancy patterns [15]–[18]. Nevertheless, unlike in static environments, occupancy is not the only information that can be extracted in dynamic environments. Supplementing additional information about the dynamics of the environment could hugely benefit path planing and object detection algorithms [11], [19]. For this purpose, information rich maps can be developed by modeling the uncertainty of directions, speed, texture, etc. of all locations of the environment in addition to occupancy information. Consider an instance as in Fig. 1 (a) where simulated humans walking in roadsides and a crosswalk. If the robot knows about the angles people turn, path planning algorithms can be designed to plan ahead and to make efficient and safer maneuvers. As shown in Fig. 1b, in this paper, we propose a novel technique to model directional uncertainty of the environment at different locations observed overtime.

[20] proposed to model human walking paths by introducing a Gaussian process prior over directions and thereby implicitly constructing a field representation of angular movements. This formulation has three main limitations: 1) because the angle is assumed to be $(-\infty, +\infty)$, predicted angles can be totally invalid, 2) it is assumed that movements at a given location occur in only one direction which is not practical for robotics applications as the robot, human, or vehicles in the environment could move in any direction, and 3) being a Bayesian nonparametric model, the algorithm becomes slower as more data are captured. On the other hand, the objective of all these approaches is to make short-term future predictions such as tracking rather than building information rich long-term maps that can be used for path planning or navigation.

In our approach, highlighting the importance of dispersion of data, the directions are represented by a probability distribution that, 1) has a valid support of $[-\pi, \pi]$ and 2) can model multi-directional movements. Having a finite number of distributions laid over the longitude-latitude space using a grid, it is possible to infer the probability of motion for any direction for each such location. This directional information can be plausibly used to extract paths as well as variously regulate path planners to avoid high risk areas or to follow the direction of traffic. Although incorporation of such probability distribution into control algorithms is beyond the focus of this paper, recent techniques have shown how to embed probability distributions to improve path planning and navigation [21]–[24]. Further, incorporating such prior information is the key in Bayesian statistical methods and prior information can be effectively used in online learning in robotics [14], [25]. Additionally, such probabilistic models naturally account for noises and imperfections in sensors and pre-processing algorithms.

Despite the importance of modeling the stochasticity of angles in robotics, it has hardly been discussed previously. Therefore, introducing directional statistics into robotics to model angular data, we present a statistical method:

1) to model multi-modal directional uncertainty in dynamic environments without obtaining spurious outputs as in current methods [20];
2) to quantitatively analyze spatial variations, temporal variations, and spatiotemporal variations;
3) that does not require heuristic parameter tuning i.e. ready for real world usage without any significant modifications

Having discussed the motivation for our work in Section I, Directional Statistics are introduced in Section II as preliminaries for the following sections. Data preprocessing steps required for mapping is detailed in Section III-A. Then, the basic method is introduced in Section III-B assuming that all movements are almost uni-directional such as one-way roads. Next, in Section III-C, theory is generalized to model multi-directional movements i.e. when there are no definite paths or dynamic objects can move in arbitrary directions such as in indoor environments or sidewalks. Experimental results are reported in Section IV followed by discussions and conclusions in Sections V and VI, respectively.

II. DIRECTIONAL STATISTICS

In this section, we introduce directional statistics where observations lie on a circle of unit radius, or in high dimensional scenarios, on a hypersphere of unit vector in the plane [3]. In order to deal with circular data, directional statistics was initially developed in physics and astronomy [26] [27], and have successful applications in meteorology [28], biostatistics [29] etc.

Although there are several approaches to model directional data, we opted for the von Mises distribution [26] because, i) it has all advantages of exponential family of distributions, ii) analogous to a Gaussian distribution with more intuitive parameters, and iii) *sufficient statistics* can be obtained explicitly [3]. These properties will be intermittently discussed in Sections III and V. The probability density function of the von Mises distribution is given by (1),

$$\mathcal{VM}(\theta; \mu, \kappa) := \frac{1}{2\pi J_0(\kappa)} \exp\big(\kappa \cos(\theta - \mu)\big), \quad (1)$$

where μ is the mean direction parameter (analogous to mean in a Gaussian distribution) and κ is the concentration parameter (weakly analogous to the reciprocal of variance in
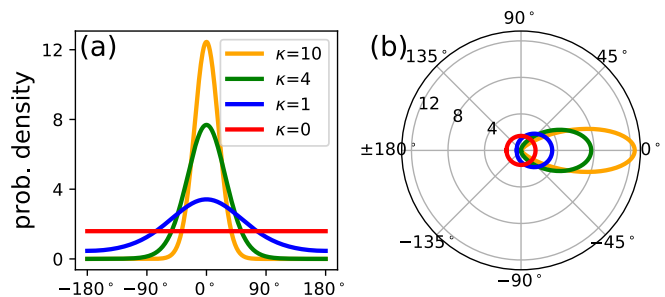

Fig. 2: The probability density functions of von Mises directional distribution (a) The effect of the concentration parameter κ for a fixed mean $\mu = 0°$. The support of von Mises distribution is $[-\pi, \pi]$. For instance, when estimating the direction of a moving object from noisy sensor measurements, a conventional Gaussian distribution which has a support $(-\infty, \infty)$ cannot be used because the actual range of directions is $[-\pi, \pi]$. (b) Corresponding polar plots.

a Gaussian distribution). $J_0(\kappa)$ is the 0th order and 1st kind modified Bessel function given by (2),

$$J_0(\kappa) := \sum_{p=0}^{\infty} \frac{1}{p!^2}\left(\frac{\kappa}{2}\right)^{2p}. \tag{2}$$

Together with the cosine term in (1), the modified Bessel function attenuates the function and keeps the support in $[-\pi, \pi]$. The effect of the κ parameter is illustrated in Fig. 2.

Considering a dataset with N directions $\mathcal{D} = \{\theta_i\}_{i=1}^N$, let us define the mean directional components,

$$\bar{C} := \sum_{i=1}^N \cos\theta_i \quad \text{and} \quad \bar{S} := \sum_{i=1}^N \sin\theta_i. \tag{3}$$

Then, the *mean direction* is given by,

$$\bar{\theta} = \begin{cases} \arctan(\bar{S}/\bar{C}), & \text{if } \bar{C} \geq 0 \\ \arctan(\bar{S}/\bar{C}) + \pi, & \text{otherwise} \end{cases} \tag{4}$$

and the *mean resultant length* is given by,

$$\bar{R} = \sqrt{\bar{C}^2 + \bar{S}^2}. \tag{5}$$

Note that $\bar{R} \in [0, 1]$ and the more homogeneous the directions are, the higher the $\bar{R}$ is. The *circular variance* is defined as $\bar{V} := 1 - \bar{R}$.

III. DIRECTIONAL GRID MAPS

Being analogous to occupancy grid maps [1], we introduce *directional grid maps* (DGM) in this section. To formally define, a DGM is a multi-dimensional field that maintains probability measures given by a probability density function of the directional uncertainty of the cells in a spatial lattice. With the proposed method, we answer the following questions:

1) What are the overall directions of motion in different places of the environment when observed over a period of time? i.e. longterm spatiotemporal analysis;
2) What is the overall direction of motion in the entire environment at a specific time? i.e. spatial analysis;
3) What is the the distribution of directions of a moving object? i.e temporal analysis.

A. Pre-processing

The inputs to build an occupancy map are occupied points and the free points in line of sight of lidar [1], [8]. However, inputs to build a DGM are angle of motion at longitude-latitude locations at different time steps: $\theta(longitude, latitude, time)$. For simplicity and to be used in collateral to occupancy grid maps, we discretize the world and assign longitude-latitude pairs to the cell they belong to. Therefore, the inputs are $\theta(cell, time)$.

Depending on the sensor type, for each time frame, θ values or the optical flow can be extracted by any of the commonly used existing methods. To name a few, data association followed by direct angle estimation or Gaussian process regression [12], tracking algorithms such as Kalman filters, particle filters, mean-shift-tracking, dense optical flow, etc. [30], [31]. Once $\theta(cell, time)$ are extracted, for the computational convenience of answering questions detailed in Section III, they are stored with tracker identities, if exists, in a spatiotemporal database [32] indexed by space and time keys.

B. Learning uni-modal movements (DGM-VM)

Without loss of generality, for the sake of simplicity to introduce the method, in this section we assume the average movements in the environment occur in approximately one direction. The more general case is introduced in Section III-C.

Consider a dataset with N directions $\mathcal{D} = \{\theta_i\}_{i=1}^N$ Assuming i.i.d. of θ, the log-likelihood of the von Mises distribution introduced in (1) is given in (6),

$$\begin{aligned}
\mathcal{L}(\mu, \kappa; \mathcal{D}) &= \log\left(\prod_{i=1}^N \frac{1}{2\pi J_0(\kappa)} \exp\left(\kappa\cos(\theta_i - \mu)\right)\right) \\
&= -N\log 2\pi - N\log J_0(\kappa) + \kappa\sum_{i=1}^N \cos(\theta_i - \mu) \\
&= -N\log 2\pi - N\log J_0(\kappa) + \kappa N\bar{R}\cos(\bar{\theta} - \mu).
\end{aligned} \tag{6}$$

The objective is to learn μ and κ given $\mathcal{D}$ to maximize the log-likelihood, i.e. maximum likelihood estimate (MLE). Intuitively, for a given dataset, MLE adjusts its parameters μ and κ to set the higher values of the probability density function align with more probable data points. These optimal parameter values can be computed by (7),

$$(\mu_*, \kappa_*) = \text{argmax}\mathcal{L}(\mu, \kappa; \mathcal{D}) = \left(\bar{\theta}, A^{-1}(\bar{R})\right) \tag{7}$$

where $A(\cdot) = \frac{J_1(\cdot)}{J_0(\cdot)}$. To derive this, take the derivative of $\mathcal{L}$ w.r.t. the parameters and equate to zero,

$$\frac{\partial\mathcal{L}}{\partial\mu} = \kappa N\bar{R}\sin(\bar{\theta} - \mu) = 0 \implies \mu_* = \bar{\theta}, \tag{8}$$

$$\begin{aligned}
\frac{\partial\mathcal{L}}{\partial\kappa} &= -N\frac{J_0'(\kappa)}{J_0(\kappa)} + N\bar{R}\cos(\bar{\theta} - \mu) \\
&= -N\frac{J_1(\kappa)}{J_0(\kappa)} + N\bar{R}\cos(\bar{\theta} - \mu) \\
&= -NA(\kappa) + N\bar{R}\cos(\bar{\theta} - \mu). \tag{9}
\end{aligned}$$

Setting $\frac{\partial\mathcal{L}}{\partial\kappa} = 0$ and $\mu_* = \bar{\theta} \implies \kappa_* = A^{-1}(\bar{R})$. See appendix for approximating $A^{-1}(\cdot)$. Alternatively, it is also possible to maximize (6) w.r.t. the parameters using stochastic gradient descent.

C. Learning multi-modal movements (DGM-VMM)

The method in section III-B assumes that movements occur only in one direction. Although this assumption might be applicable for roads with vehicles running in dedicated lanes, such an assumption is not generally suitable for crosswalks, sidewalks, manipulators, or aerial vehicles (Fig. 3). Therefore, in order to capture multi-directional movements, we use the convex combination of a mixture of M directional distributions. The probability density function of such a mixture with M von Mises distributions is given by (10).

$$\mathcal{VMM}(\theta; \alpha, \mu, \kappa) := \sum_{m=0}^M \alpha_m \mathcal{VM}(\theta; \mu_m, \kappa_m), \tag{10}$$

$$\kappa_m = A^{-1}\left(\frac{\|\sum_{n=1}^{N}\gamma_{mn}\theta_n\|}{\sum_{n=1}^{N}\gamma_{mn}}\right), \qquad (14)$$

where $A^{-1}(\cdot)$ is the inverse of Bessel function ratios as described in Section III-B.

Algorithm 1: EM algorithm for multi-modal learning. *CalcRes()* and *UpdateParameters()* are (11) and (12)-(14), respectively.

Input: $\{\theta_n\}_{n=1}^{N}$
$\{\mu_m^{(0)}\}_{m=1}^{?}$ = DBSCAN(θ) //get density centers;
M =size($\{\mu_m^0\}$) //number of mixture components;
Initialize $\alpha_m^{(0)} = 1/M$, for $m = 1 : M$;
Initialize $\kappa_m^{(0)} \gtrsim +0$, for $m = 1 : M$;
Initialize $\epsilon \approx +0$;
Initialize $i = -1$ //iterations;
while $\|\mu_m^{(i)} - \mu_m^{(i-1)}\| \leq \epsilon$ **do**
  $i \leftarrow i + 1$;
  //E-step;
  for $n = 1$ *to* N **do**
    for $m = 1$ *to* M **do**
      $\hat{\gamma}_{mn}^{(i)}$ =*CalcRes*$\big(\theta_n, \alpha_m^{(i-1)}, \mu_m^{(i-1)}, \kappa_m^{(i-1)}\big)$;
    end
  end
  //M-step;
  for $m = 1$ *to* M **do**
    $\big(\alpha_m^{(i)}, \mu_m^{(i)}, \kappa_m^{(i)}\big)$ =*UpdateParameters*$\big(\hat{\gamma}_{mn}^{(i)}\big)$;
  end
end
Output: $\alpha_m^{(i)}, \mu_m^{(i)}, \kappa_m^{(i)}$ //$\mathcal{VMM}$ (10)

IV. EXPERIMENTS

A. Experimental setup and evaluation metrics

As given in Table I, we used a variety of datasets from simulated and real-world environments having both LiDAR and cameras, to validate different aspects of the proposed methods and answer questions raised in Section III.

In order to assess models, we used several metrics. In a M-mixture of distributions, the expected negative log-likelihood (ENLL) is calculated as the average negative log-likelihood over all data points[39] which indicates the likelihood a given data point sampled from the distribution parameterized by $\{(\mu_{m*}, \kappa_{m*})\}_{m=1}^{M}$. For unimodal settings $M = 1$. The smaller the NLL or ENLL, the better the model fit is.

As a another metric, average probability density (APD) is considered. Metrics are calculated with a 10-fold cross-validation procedure. For each fold of test data, the probability density is calculated and averaged. Intuitively, if the model has captured the full long-term distribution, it gives a higher APD score because more points are concentrated around the vicinity if that area. Unfortunately, because of the problem is unsupervised learning and having a mixture of distributions, most of the standard tests that are commonly
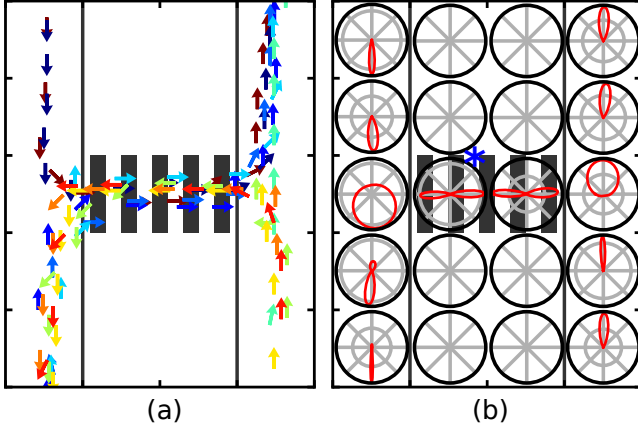

Fig. 3: Mapping multi-modality. (a) More human paths are added to Fig. 1 so that human walk in different directions in some places e.g. crosswalk (b) DGM modeled using the mixture of von Mises distributions. With comparison to Fig. 1 (a) which only has a single von Mises distribution, observe that some cells in (b) have two lobes indicating the method's capacity to learn bimodal movements. The middle-left cell shows a more circular distribution because movements occur in different directions.

with $\sum_{m=0}^{M}\alpha_m = 1$ for $\alpha_m \geq 0$ to guarantee $\mathcal{VMM}$ is a valid probability density function.

However, there is no closed-form solution to find the optimal parameter set $\{(\alpha_m, \mu_m, \kappa_m)\}_{m=1}^{M}$. Therefore, as with Gaussian mixture models, Expectation-Maximization (EM) algorithm can be used [33]. This is an iterative procedure where the posterior is estimated using the parameters estimated in the previous iteration, and the parameters are updated using the estimated posterior in the current iteration. Once the parameters do not significantly change over iterations, the optimization procedure can be stopped. This is detailed in Algorithm 1.

The naive EM algorithm only learns the parameters, not the number of mixture components M. Although it is possible to preset it as a fixed number, in order to make the algorithm faster and to make mapping fully autonomous, we made use of DBSCAN [34] clustering technique and initialized $\{\mu_m\}_{m=1}^{M}$ with cluster centers, and then optimized using the EM algorithm. Unlike the popular k-means algorithm where the user requires to provide the number of clusters, DBSCAN determines it using the density of data points which is indeed our requirement.

In a similar fashion to a Gaussian mixture model [35], in the E-step, the elements of the responsibility matrix are computed as in (11).

$$\gamma_{mn} = \frac{\alpha_m \mathcal{VM}_m(\theta_n)}{\sum_{m'=1}^{M}\alpha_{m'}\mathcal{VM}_{m'}(\theta_n)}, \qquad (11)$$

where $\mathcal{VM}_m$ indicates a von Mises probability density function of the mixture component m. Having obtained γ_{mn}, the objective of the M-step is to learn the parameters using (12)-(14),

$$\alpha_m = \frac{\sum_{n=1}^{N}\gamma_{mn}}{N}, \qquad (12)$$

$$\mu_m = \frac{\sum_{n=1}^{N}\gamma_{mn}\theta_n}{\|\sum_{n=1}^{N}\gamma_{mn}\theta_n\|}, \qquad (13)$$

TABLE I: Description of datasets

Datasets	Description
Unimodal	Similar to [20], this simulated dataset represents human walking paths which collectively have a **unimodal** directional pattern i.e. at a given location all human walk approximately in the same direction. Observations are assumed to be taken from the top view. (Fig. 1 (a))
Multi-modal	This is the **multi-modal** (to be exact, bi-modal) extension to the above unimodal dataset. (Fig. 3 (a))
Edinburgh	The publicly available **Edinburgh** Informatics Forum Pedestrian Database (Aug.24) [36] is used. The setup is an highly dynamic outdoor environment with RGB cameras setup on top to track [36] people. (Fig. 5 (a))
Kuka	Here, we use the **Kuka** robot arm in the MORSE simulator [37]. The location of the end-effector in the 2D space was tracked. Using only two joints, we manipulated the robot to make planar movements to simulate a repetitive task with normally distributed random perturbations to the goal locations. Because of this perturbations, robot's path is slightly different in each of the 20 iterations which results in observing different angles of the end effector in the same location. (Fig. 6 (a))
Corridor	This tracks five people moving in a **corridor** using a moving robot with a LiDAR [38]. (Fig. 8 (a))
Intersection	This is similar to the corridor dataset, however in a four-way **intersection** (Fig. 9 (a))
Human	The single trajectory of a walking **human** in a MORSE-simulated office environment is tracked. (Fig. 10 (a))

used in linear statistics and robotics with normality assumptions cannot be used for this setting.

A notebook computer with an Intel Core-i7 processor and a 8 GM RAM was used for experiments. For all experiments, the tolerance parameter of the VMM algorithm ϵ and the density parameter of the DBSCAN were set to 10^{-6} and 0.5, respectively. When using the Edinburgh dataset with Gaussian process [20] is used in comparisons, a low-rank approximation [40] had to be used because the Edinburgh dataset contains 76260 data points which is not feasible to fit using the full Gaussian process model. The python code will be available soon: github.com/RansML.

B. Experiment 1: Validating the EM algorithm

Firstly, we show that the iterative EM algorithm described in Section III-C in deed minimizes the NLL over the number of iterations. In Fig. 4, NLL is plotted against the number of iterations for the cell marked with "∗" in Fig. 3 (b) for the multi-modal dataset. For the Multi-modal dataset, the EM algorithm converged within 5 iterations. The mean squared error (MSE) of angles is reported in Table III. In DGM-VMM, the MSE to the closest mode was considered.
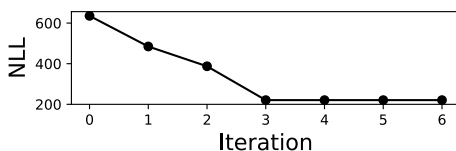

Fig. 4: Convergence of the EM algorithm

TABLE II: Mean squared error (MSE) of angles.

Method	Unimodal	Multi-modal
DGM-VMM	**0.231**	**1.100**
DGM-VM	0.239	2.484

C. Experiment 2: Modeling long-term spatiotemporal effects

In this section, we used Unimodal, Multi-modal, Edinburgh, and Kuka datasets to build the long-term spatiotemporal directional grid map so as to answer the question "What are the directions of movements in different places of the environment when observed over a period of time?". The resolutions of the grid maps were kept constant for demonstration and visualization purposes (5×4, 5×4, and 17×23 cells for Unimodal, Multimodal, and Edinburgh datasets). The maps for Unimodal and Multimodal datasets are shown in Fig. 1 (b) and 3 (b), respectively. Around 15% of randomly selected trajectories are shown in Fig. 5 (a) and the corresponding DGM in Fig. 5 (b). By comparing the trajectories and directions of lobes with intensities, it is possible to see the model has successfully learned the directions, including multi-modality. In order to demonstrate that the proposed algorithm is well suitable for other domains, we used the Kuka dataset. Additionally, as shown in Fig. 6 (b), rather than maintaining a fixed grid, observations were taken from a few user specified locations in the space.

The quantitative aspects of different methods are given in Table III. DGM-VMM is faster because 1) its means are initialized from DBSCAN, and 2) it has the flexibility to adjust to any shape. For the Unimodal dataset, the Gaussian process based method proposed in [20] works well. As illustrated in Fig 7, because the Gaussian process cannot handle multi-directional data, it merely averages directions, resulting in incorrect predictions.

D. Experiment 3: Analyzing spatial variations

This is merely a demonstration to show that the same model can be used to answer "at a given time, where do everyone in the environment move?" For this purpose, all data points at a given time (i.e. $t =$fixed and all cells) in the Edinburgh dataset were considered and the EM algorithm was run for the von Mises mixture. The resulting polar plot is shown in Fig. 5 (c). To interpret, considering the entire environment, many people move towards $\approx -90°$ and a few people $\approx 90°$. This kind of an analysis provides a summary statistic about the environment at a given time. Further, it is also possible to answer questions such as how fast the distribution changes over time by quantifying using a mutual information or KullbackLeibler divergence.

E. Experiment 4: Analyzing temporal variations

In this experiment, we analyze the temporal evolution of dynamic objects individually. For this purpose, we used the Corridor and Intersection datasets, and corresponding directional distributions are found in Figs. 8 and 9, respectively.

Then, using the Human dataset, temporal evolution of the map was analyzed in a sequential learning setting. In the
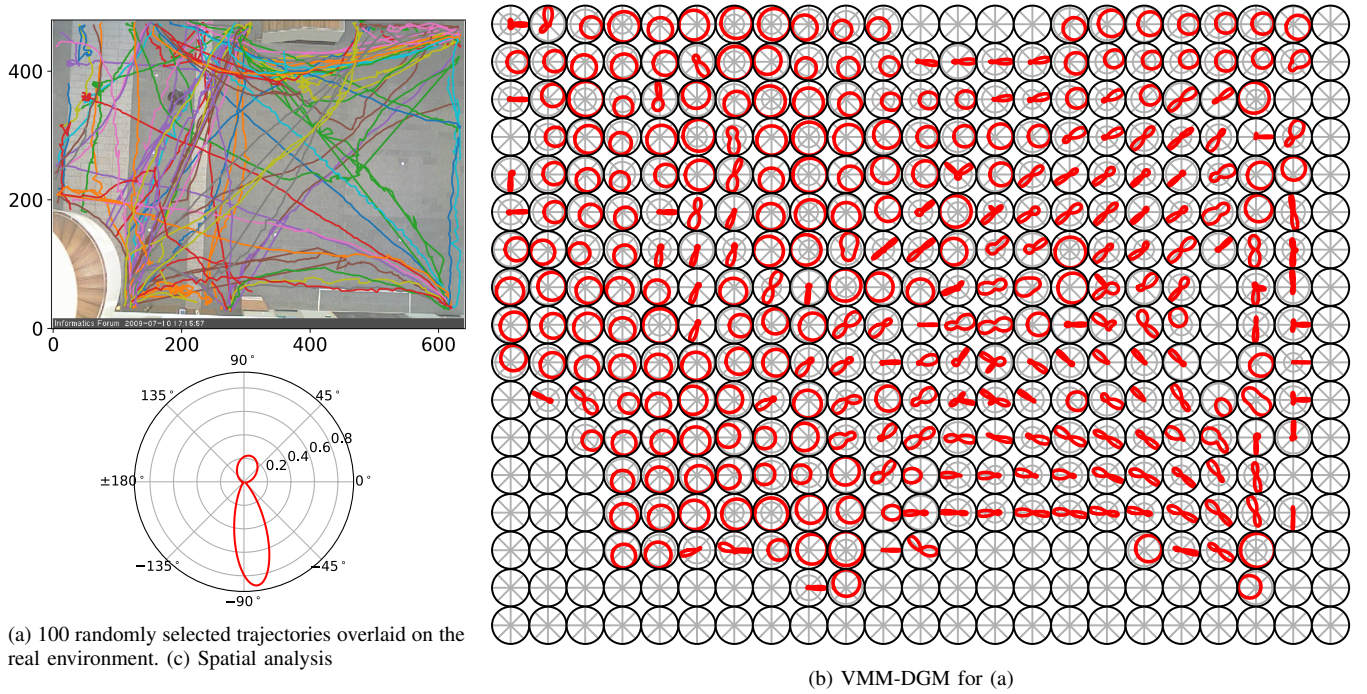
(a) 100 randomly selected trajectories overlaid on the real environment. (c) Spatial analysis

(b) VMM-DGM for (a)

Fig. 5: Edinburgh pedestrian dataset shows how people near the University of Edinburgh's Atrium move from one building to another on a regular day.

TABLE III: Performance metrics for different methods. The smaller the ENLL or the higher the APD, the better the model is.

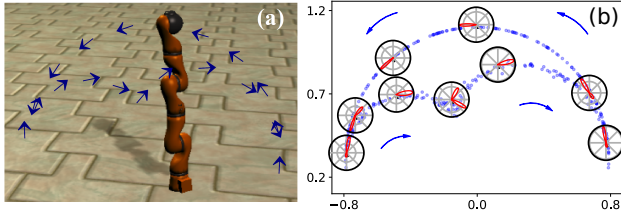| Method	Unimodal dataset			Multimodal dataset			Edinburgh dataset			Kuka dataset		
	ENLL	APD	Time	ENLL	APD	Time	ENLL	APD	Time	ENLL	APD	Time
DGM-VMM	**0.113**	1.358	**15±13**	**0.251**	**1.015**	**33±27**	**1.483**	**0.251**	**28±25**	-0.087	**1.190**	**13±9**
DGM-VM	0.177	1.172	71±34	0.696	0.615	115±62	1.733	0.202	72±72	0.747	0.699	55±15
GP [20]	N/A	**1.711**	278±16	N/A	0.211	213±120	N/A	0.124	>3600	N/A	0.217	413±40

Fig. 6: The Kuka robot arm (a) The approximate path of the end-effector is shown in blue arrows. Directional map of the Kuka end-effector movements. (b) Some of the data points collected over 20 such cycles with perturbation are shown in blue dots. The corresponding directional distribution at arbitrary locations are indicated by ploar plots.
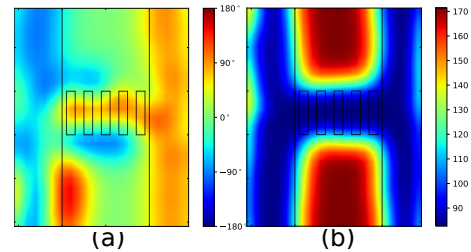

Fig. 7: Gaussian process (GP) mapping [20] for Multimodal dataset where movements occur in different directions. This can be compared with Fig. 3. (a) mean direction (b) confidence as variance. Observe that the predictions around places where multi-directional movements occur i.e. crosswalk and lower-left sidewalk is not accurate. In such places the GP averages all directions. As shown in (b), despite the inaccurate predictions the confidence about the prediction in such areas is also very high. Although angles are limited to $[-180°, 180°]$ in the figure, they can be in the range $(-\infty°, \infty°)$ without satisfying the recurrence relationship $f(\theta) = f(\theta + 360°)$.

office environment shown in Fig 10 (a), the trajectory of a simulated human is shown in Fig 10 (b). The model is learned in an online fashion as data are collected over 286 times steps. In Fig 10 (c), the directional distribution of four such time steps are shown. Starting with a dispersed distribution (i.e. any angle is possible or $\kappa \approx 0$), the observing robot sequentially learns the directions the human moves.

V. DISCUSSIONS

Similar to a Gaussian distribution, the mean, mode, and median of a unimodal von Mises is the same. However, when a mixture of von Mises is considered these quantities can be different. Especially, for practical applications, it is important to determine the modes. This is not straightforward because the values of κ and μ determines both the number of modes and where they are. However, because von Mises belongs to the exponential family of distributions, it is possible to utilize similar algorithms that are used to find modes in mixture of Gaussians [41] or wavelet based methods used in signal processing to find peaks [42].

In the proposed algorithm, we used DBSCAN to determine the number of mixture components. As this is not part of the EM algorithm, the number of mixture components
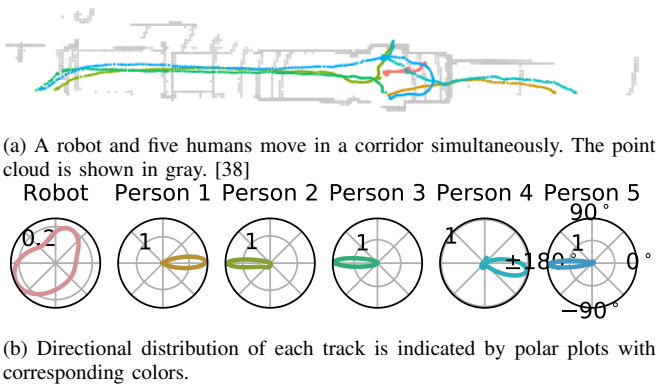
(a) A robot and five humans move in a corridor simultaneously. The point cloud is shown in gray. [38]

(b) Directional distribution of each track is indicated by polar plots with corresponding colors.

Fig. 8: Corridor dataset

(a) Five humans move in an intersection simultaneously. The point cloud is shown in gray. [38]

(b) Directional distribution of each track is indicated by polar plots with corresponding colors.
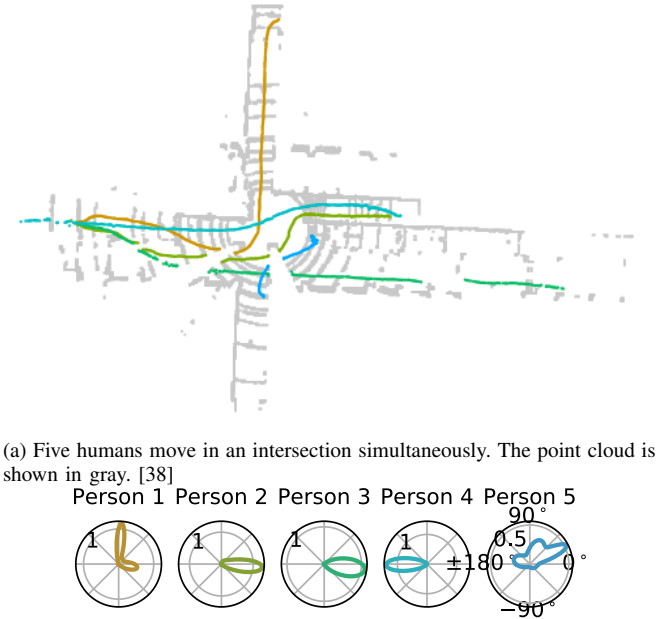
Fig. 9: Intersection dataset.

maybe suboptimal. In order to further improve the likelihood, especially in high dimensional settings or when there is a small amount of data, taking a Bayesian approach, it is possible to consider M as a parameter to be learned. Taking further advantages of the exponential family of distributions, as with mixture of Gaussians [35], it can be easily factorized and apply variational inference to jointly learn the number of mixtures as well as mixture parameters.

The one dimensional formulation can be easily extended to higher dimensions using the von Mises-Fisher extension given by 15 for $(D-1)$ dimensions,

$$\mathcal{VM}_D(\theta; \mu, \kappa) := \frac{\kappa^{D/2-1}}{(2\pi)^{D/2} J_{D/2-1}(\kappa)} \exp\left(\kappa \mu^\top \theta\right). \quad (15)$$

Such an extension can be used in modeling 3D spatiotemporal dynamics or modeling joint rotational uncertainties in robot manipulators with high degrees of freedom. By modeling bi-directional 3D uncertainties of a toy dataset (e.g. a moving drone in 3D), Fig. 11 (b) illustrates that such an extension is straightforward.

(a) A person walking in the office environment.

(b) The plain view of the trajectory.

(c) The directional distribution for four tome steps. Initially, it is a uniform circular distribution. Observe how the direction of lobes changes with the direction of trajectories at different time steps.
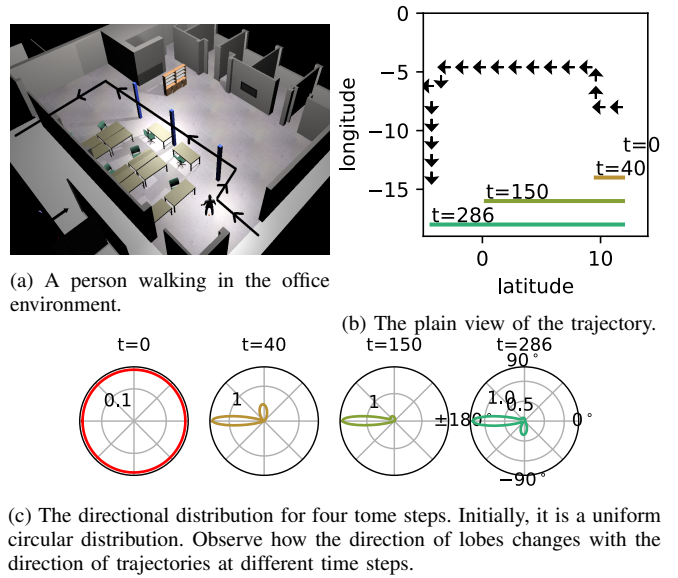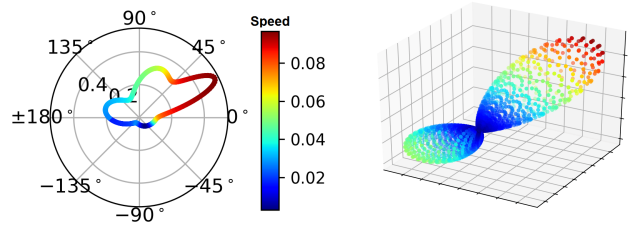
Fig. 10: Human dataset

Fig. 11: Usefulness of DGM (a) The directional distribution of Person 5 in Fig. 9 with colors indicating different speeds i.e. speed for different angles with the probability of angle (b) Demonstration of 3D lobes modeled using the von Mises-Fisher distribution.

Interestingly, it is possible to use these directional maps along with other information extracted from dynamic environments to build maps that are informative. For instance, Fig. 11 (a) shows speeds (separately modeled) of different directions of "Person 5" in Fig. 9. Additionally, a large DGM can be easily bundled together with a occupancy grid map to represent the dynamics of the environment well. These information rich maps can then be used to make planning algorithms robust [21], [23].

One of the main limitations of the proposed method, as with any other grid based method [1], the independence assumption among cells [8]. Therefore, it might be useful to consider the directional distribution as a conditional distribution or to have a more continuous representation [14], [43].

VI. CONCLUSIONS

We presented a robust algorithm to estimate angular uncertainties ubiquitous in robotics. To this end, we effectively we made use of directional statistics that are not typically utilized in robotics. Our method is generic enough to be used in any robotic platform such as mobile robots, drones, manipulators, etc. or in a variety of domains such as indoor mapping, field robotics, and human-robot interaction.

APPENDIX

To evaluate κ_* using $A^{-1}(\cdot)$,

$$\kappa_* \approx \begin{cases} 2\bar{R} + \bar{R}^3 + \frac{5}{6}\bar{R}, & \text{for small } \bar{R} \\ 0.5(1-\bar{R})^{-1}, & \text{otherwise} \end{cases}$$

For empirical values of "small," refer [3], [27].

REFERENCES

[1] A. Elfes, "Sonar-based real-world mapping and navigation," *IEEE Journal of Robotics and Automation*, vol. RA-3(3), pp. 249–265, 1987.

[2] F. Ramos and L. Ott, "Hilbert maps: scalable continuous occupancy mapping with stochastic gradient descent," in *Proceedings of Robotics: Science and Systems (R:SS)*, Rome, Italy, July 2015.

[3] K. V. Mardia and P. E. Jupp, *Directional statistics*. New York: Wiley. Merrifield, 2006.

[4] P. Henry, M. Krainin, E. Herbst, X. Ren, and D. Fox, "Rgb-d mapping: Using kinect-style depth cameras for dense 3d modeling of indoor environments," *The International Journal of Robotics Research (IJRR)*, vol. 31, no. 5, pp. 647–663, 2012.

[5] J. Bohg, "Multi-modal scene understanding for robotic grasping," Ph.D. dissertation, KTH Royal Institute of Technology, 2011.

[6] J. Yin, L. Carlone, S. Rosa, and B. Bona, "Graph-based robust localization and mapping for autonomous mobile robotic navigation," in *Mechatronics and Automation (ICMA), 2014 IEEE International Conference on*. IEEE, 2014, pp. 1680–1685.

[7] A. Hornung, K. M. Wurm, M. Bennewitz, C. Stachniss, and W. Burgard, "Octomap: An efficient probabilistic 3d mapping framework based on octrees," *Autonomous Robots*, vol. 34, no. 3, pp. 189–206, 2013.

[8] S. T. O'Callaghan and F. T. Ramos, "Gaussian process occupancy maps," *The International Journal of Robotics Research (IJRR)*, vol. 31, no. 1, pp. 42–62, 2012.

[9] D. Hahnel, R. Triebel, W. Burgard, and S. Thrun, "Map building with mobile robots in dynamic environments," in *IEEE International Conference on Robotics and Automation (ICRA)*, 2003, pp. 4270–4275.

[10] W. Burgard, C. Stachniss, and D. Hähnel, "Mobile robot map learning from range data in dynamic environments," in *Autonomous Navigation in Dynamic Environments*. Springer, 2007, pp. 3–28.

[11] A. Walcott-Bryant, M. Kaess, H. Johannsson, and J. J. Leonard, "Dynamic pose graph slam: Long-term mapping in low dynamic environments," in *Intelligent Robots and Systems (IROS), 2012 IEEE/RSJ International Conference on*. IEEE, 2012, pp. 1871–1878.

[12] R. Senanayake, L. Ott, S. O'Callaghan, and F. Ramos, "Spatio-temporal hilbert maps for continuous occupancy representation in dynamic environments," in *Neural Information Processing Systems (NIPS)*, 2016.

[13] R. Senanayake, S. O'Callaghan, and F. Ramos, "Learning highly dynamic environments with stochastic variational inference," in *IEEE International Conference on Robotics and Automation (ICRA)*, 2017.

[14] R. Senanayake and F. Ramos, "Bayesian hilbert maps for dynamic continuous occupancy mapping," in *Conference on Robot Learning (CoRL)*, 2017, pp. 458–471.

[15] J. Saarinen, H. Andreasson, and A. Lilienthal, "Independent Markov Chain Occupancy Grid Maps for Representation of Dynamic Environment," in *IEEE/RSJ International Conference on Intelligent Robots and Systems (IROS)*, 2012, pp. 3489–3495.

[16] D. Meyer-Delius, M. Beinhofer, and W. Burgard, "Occupancy Grid Models for Robot Mapping in Changing Environments," in *proc. AAAI Conference on Artificial Intelligence (AAAI)*, 2012, pp. 2024–2030.

[17] Z. Wang, P. Jensfelt, and J. Folkesson, "Modeling spatial-temporal dynamics of human movements for predicting future trajectories," in *AAAI Conference on Artificial Intelligence (AAAI)*, 2015, pp. 42–48.

[18] T. Krajník, P. Fentanes, G. Cielniak, C. Dondrup, and T. Duckett, "Spectral analysis for long-term robotic mapping," in *IEEE International Conference on Robotics and Automation (ICRA)*, 2014, pp. 3706–3711.

[19] N. Bore, "Object instance detection and dynamics modeling in a long-term mobile robot context," Ph.D. dissertation, KTH Royal Institute of Technology, 2017.

[20] S. T. O'Callaghan, S. P. Singh, A. Alempijevic, and F. T. Ramos, "Learning navigational maps by observing human motion patterns," in *Robotics and automation (ICRA), 2011 IEEE international conference on*. IEEE, 2011, pp. 4333–4340.

[21] Z. Marinho, B. Boots, A. Dragan, A. Byravan, G. J. Gordon, and S. Srinivasa, "Functional gradient motion planning in reproducing kernel hilbert spaces," in *Proceedings of Robotics: Science and Systems (R:SS)*, 2016.

[22] J. Dong, M. Mukadam, F. Dellaert, and B. Boots, "Motion planning as probabilistic inference using gaussian processes and factor graphs." in *Robotics: Science and Systems (R:SS)*, vol. 12, 2016.

[23] M. Norouzii, J. V. Miro, and G. Dissanayake, "Probabilistic stable motion planning with stability uncertainty for articulated vehicles on challenging terrains," *Autonomous Robots*, vol. 40, no. 2, pp. 361–381, 2016.

[24] M. Mukadam, J. Dong, F. Dellaert, and B. Boots, "Simultaneous trajectory estimation and planning via probabilistic inference," in *Proceedings of Robotics: Science and Systems (R:SS)*, 2017.

[25] T. D. Bui, C. Nguyen, and R. E. Turner, "Streaming sparse gaussian process approximations," in *Advances in Neural Information Processing Systems*, 2017, pp. 3301–3309.

[26] R. von Mises, "Über die 'ganzzahligkeit' der atomgewichte und verwandte fragen," *Phys. Z*, vol. 19, no. 490-500, 1918.

[27] K. V. Mardia and R. Edwards, "Weighted distributions and rotating caps," *Biometrika*, vol. 69, no. 180, pp. 323–330, 1982.

[28] M. S. Handcock and J. R. Wallis, "An approach to statistical spatial-temporal modeling of meteorological fields," *Journal of the American Statistical Association*, vol. 89, no. 426, pp. 368–378, 1994.

[29] J. L. van Hemmen, "Vector strength after goldberg, brown, and von mises: biological and mathematical perspectives," *Biological cybernetics*, vol. 107, no. 4, pp. 385–396, 2013.

[30] G. Farnebäck, "Two-frame motion estimation based on polynomial expansion," in *Image Analysis*. Springer, 2003, pp. 363–370.

[31] S. Sivaraman and M. M. Trivedi, "Looking at vehicles on the road: A survey of vision-based vehicle detection, tracking, and behavior analysis," *IEEE Transactions on Intelligent Transportation Systems*, vol. 14, no. 4, pp. 1773–1795, 2013.

[32] R. H. Güting and M. Schneider, *Moving Objects Databases*. Morgan Kaufmann, 2005.

[33] I. S. Dhillon and S. Sra, "Modeling data using directional distributions," Technical Report TR-03-06, Department of Computer Sciences, The University of Texas at Austin., Tech. Rep., 2003.

[34] M. Ester, H.-P. Kriegel, J. Sander, X. Xu, *et al.*, "A density-based algorithm for discovering clusters in large spatial databases with noise." in *ACM SIGKDD Conference on Knowledge Discovery and Data Mining (KDD)*, vol. 96, no. 34, 1996, pp. 226–231.

[35] C. Bishop, *Pattern Recognition and Machine Learning*. Springer, 2006.

[36] B. Majecka, "Statistical models of pedestrian behaviour in the forum," *Master's thesis, School of Informatics, University of Edinburgh*, 2009.

[37] G. Echeverria, S. Lemaignan, A. Degroote, S. Lacroix, M. Karg, P. Koch, C. Lesire, and S. Stinckwich, "Simulating complex robotic scenarios with morse," in *Simulation, Modeling, and Programming for Autonomous Robots (SIMPAR)*, 2012, pp. 197–208.

[38] C. Romero-González, Á. Villena, D. González-Medina, J. Martínez-Gómez, L. Rodríguez-Ruiz, and I. García-Varea, "Inlida: A 3d lidar dataset for people detection and tracking in indoor environments." in *Proceedings of the 12th International Joint Conference on Computer Vision, Imaging and Computer Graphics Theory and Applications (VISIGRAPP)*, 2017, pp. 484–491.

[39] D. Ruppert, *Statistics and data analysis for financial engineering*. Springer, 2011, vol. 13.

[40] GPy, "GPy: A gaussian process framework in python," http://github.com/SheffieldML/GPy, since 2012.

[41] M. A. Carreira-Perpinan, "Mode-finding for mixtures of gaussian distributions," *IEEE Transactions on Pattern Analysis and Machine Intelligence*, vol. 22, no. 11, pp. 1318–1323, 2000.

[42] P. Du, W. A. Kibbe, and S. M. Lin, "Improved peak detection in mass spectrum by incorporating continuous wavelet transform-based pattern matching," *Bioinformatics*, vol. 22, no. 17, pp. 2059–2065, 2006.

[43] L. McCalman, S. O'Callaghan, and F. Ramos, "Multi-modal estimation with kernel embeddings for learning motion models," in *Robotics and Automation (ICRA), 2013 IEEE International Conference on*. IEEE, 2013, pp. 2845–2852.